AALBORG UNIVERSITY

Voltage Ride through Control Strategy of Modular Multilevel Converter under Unbalanced Voltage Sag

Hakimi, Seyed Mehdi ; Hajizadeh, Amin

Link to publication from Aalborg University

Article

Voltage Ride through Control Strategy of Modular Multilevel Converter under Unbalanced Voltage Sag

Seyed Mehdi Hakimi [1] and Amin Hajizadeh [2],*

[1] Department of Electrical Engineering, Damavand Branch, Islamic Azad University, 39718-78911 Damavand, Iran; sm_hakimi@damavandiau.ac.ir
[2] Department of Energy Technology, Aalborg University, 6700 Esbjerg, Denmark
* Correspondence: aha@et.aau.dk, Tel.:+459-940-7746

check for
updates

Abstract: This paper develops modeling and describes a control strategy for a modular multilevel converter (MMC) for grid-connected renewable energy systems. The proposed model can be used to simulate MMC activity during normal and faulty situations. Firstly, a dynamic model of a grid-connected MMC (GC-MMC), based upon the symmetrical component of voltages and currents, was designed. Then an adaptive robust control approach was established in order to follow the reference currents of the converter and stabilize the submodule (SM) capacitor voltage. The positive and negative sequences of reference currents that were given from the demanded active and reactive power during grid voltage disturbance and a normal situation were then utilized in control loops. Finally, the numerical results for the performance of the MMC throughout voltage sag conditions and the effect of uncertainties on the filter parameters during changing power demands were evaluated. The results specified that the current control strategy is more potent under voltage sag situations and able to fulfill the stability requirements of the MMC.

Keywords: control; modeling; MMC; unbalanced voltage

1. Introduction

Recently, the modular multilevel converter (MMC) has gained more importance for different applications such as high-voltage direct current (HVDC) and renewable power generation systems [1,2]. They can provide high reliability and good harmonic performance in grid-connected converters [3]. In the structure of an MMC, a high number of semiconductor switches and capacitors are employed. A small part of the active power is absorbed by the MMC to retain the voltage of the submodule (SM) capacitors constant as well as compensate the active power losses. However, the voltage of the capacitor can create an imbalance due to a mismatch in conduction and the switching power losses. Balancing the SM capacitor voltages has been a major technical challenge in the latest research [4,5]. Currently, many kinds of literature on voltage balancing techniques are available. These can be sorted into distributed voltage control approaches and centralized SM selection control approaches [6]. Both contain controlling capacitor voltages based on the control of power electronic switches during the controlled pre-charge and normal operation stages of the power system [7]. Moreover, there have been investigations regarding the execution of an advanced current controller for the MMC.

A combination of model predictive control (MPC) and classical control has previously been presented [8] for the MMC's voltages balancing. In this approach, an arranging method is utilized to accomplish SM capacitor voltage balancing and other control objectives are realized with an MPC strategy. Thus, the number of switching states and computational load on the MPC strategy is considerably reduced [9]. However, the computational complication is one of the main matters in MPC. A new capacitor static voltage balance method based on self-power supply control has been

presented elsewhere [10]. In this technique, the SM capacitor voltages are organized from low to high and the minimum SM capacitor voltage is controlled by the regulating of the self-power supply input current. However, the time required for voltage balance will be longer, when an MMC has more SMs.

The literature [11–13] uses different methods to reduce the capacitance-voltage deviation between SMs. In Reference [14], the SM capacitor voltage was balanced by a carrier-based pulse width modulation method. This method can better reduce the capacitance-voltage deviation between SMs, but it is necessary to add a controller to each SM for control, which increases the economic cost and system complexity.

In References [15–17], if the SM capacitor voltage deviation was within the acceptable range of the system, the SM switching frequency was reduced by different methods. In Reference [16], the SM operating state was determined according to the direction of the bridge arm current and change trend of the reference voltage. In Reference [17], a method of fixing the switching frequency was proposed.

In all the aforementioned studies, an inclusive model for assessment of the MMC during unbalanced voltage conditions was absent. Therefore, it is crucial to report on the behavior of the MMC under different voltage disturbances in distribution power systems. Hence, some published studies have taken a look into the control and analysis of the renewable power generation system during faulty conditions in an unbalanced network. In Reference [11], a grid-connected wind-photovoltaic (PV) hybrid system with battery energy storages was offered in order to increase the integration proportion of renewable energies. In this study, a control strategy was developed to insulate the hybrid power system during a grid fault. Moreover, the study in Reference [12] offered a symmetrical components control algorithm, proposing it for a four-leg, three-phase, grid-connected voltage source converter used for renewable energy resources with wind–solar–battery units. A mechanism of negative and zero sequences injection based on the control of (d, q) current coordinates was introduced. The ability of the entire control system to enhance the unbalanced fault ride-through capability of the distributed power generation system was also evaluated by time domain simulations. Furthermore, in Reference [13], a shunt active power filter based on a three-level inverter was employed to reduce both the whole switching power losses and total harmonic distortion (THD). The main contribution of this study is its survey of the prospects of the multilevel inverter being involved as a shunt active filter on the control of the reactive power, as well the harmonics mitigation drawn from a nonlinear load and unbalanced sources. Therefore, an intelligent controller is recommended for a three-level shunt active filter to overcome the asymmetrical conditions on the grid voltages and control of DC link voltage.

In general, the objectives and novelties of the current study are described as follows:

- The development of a dynamic model of the grid-controlled (GC)-MMC, based on a symmetrical component of voltages and currents considering positive and negative sequences;
- The design a fuzzy-sliding model of control to regulate the symmetrical components of upper and lower arm currents and stabilize the SM's capacitor voltages;
- The improvement of the robustness and stability of the controllers; and
- Dynamic performance validation of a proposed controller for the GC-MMC under different conditions, including grid faults and normal situations, through simulation and experimental implementation.

This paper is classified as follows: Section 2 presents the modeling of the GC-MMC. Then the proposed control scheme is presented in Section 3. Finally, in Section 4, the simulation results are presented with additional details.

2. Modeling of the Grid-Connected Modular Multilevel Converter

The classic formation of an MMC that is integrated to photovoltaic (PV) units as a renewable energy source is presented in Figure 1. To explore the dynamic behavior features of a GC-MMC, a precise model is needed. In fact, the developed model in this paper is based on the average modeling technique which has been popularly used in many research papers, i.e., the accelerated

switching function model of MMCs used in Reference [18]. This model improves the simulation speed significantly and the Central Processing Unit (CPU) running time is reduced by a third for the tested two-terminal HVDC-link. This can provide significant benefits when studying large HVDC networks that involve many converter stations, as well as various operating conditions, including normal operation, AC fault, DC fault, etc. The mathematic equations of an N-cell MMC are described as follows [14]:

$$
\begin{aligned}
\frac{di_{uk}}{dt} &= \frac{1}{L}\left[\frac{V_{dc}}{2} - \sum_{i=1}^{N}\left(d_i.V_{C_{i-uk}}\right) - Ri_{uk} - V_k\right] \\
\frac{di_{lk}}{dt} &= \frac{1}{L}\left[\frac{V_{dc}}{2} - \sum_{i=N+1}^{2N}\left(d_i.V_{C_{i-lk}}\right) - Ri_{lk} + V_k\right] \\
\frac{dV_{C_{i\_uk}}}{dt} &= \frac{1}{C}\left(i_{uk}.d_i\right)i = 1,\dots,N \\
\frac{dV_{C_{i\_lk}}}{dt} &= \frac{1}{C}\left(i_{lk}.(1-d_i)\right)i = N+1,\dots,2N
\end{aligned}
\tag{1}
$$

where i_u, i_l, V_{Ci_u}, V_{Ci_l} are the upper/lower values for the arm currents and capacitor voltages, respectively. Moreover, d_i, V_{dc} and V_k are the gating signal of the upper gate of the *i*-th cell, DC-link voltage and phase *k* ={*a,b,c*} voltage, respectively.
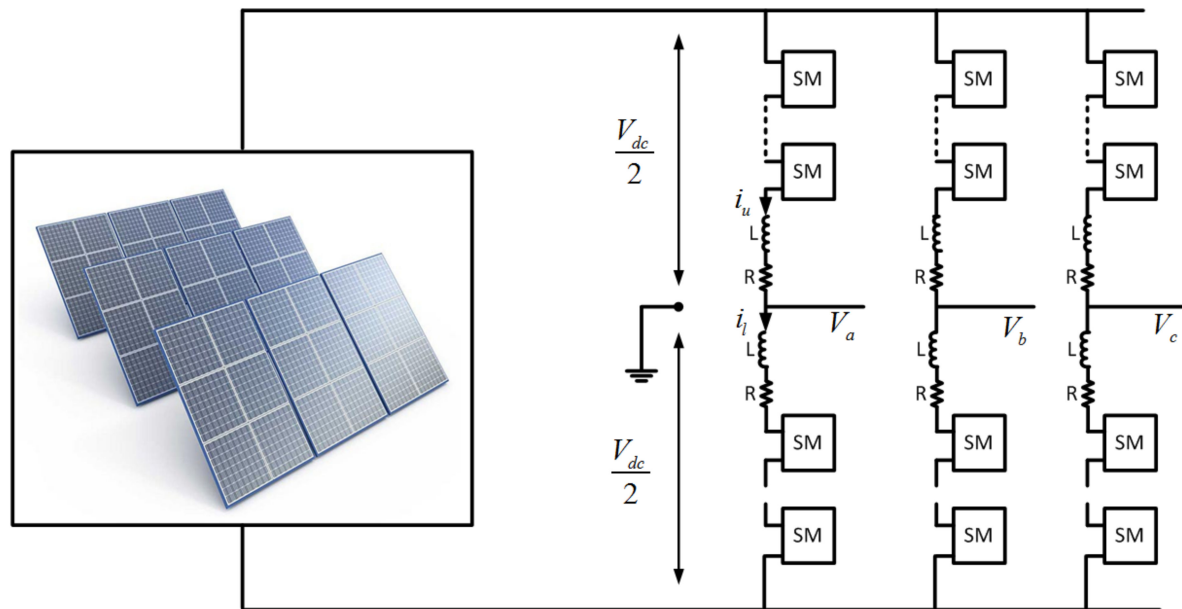

Figure 1. The circuit diagram of a classic modular multilevel converter (MMC).

The presence of unbalanced voltage disturbance in a grid leads to the utilization of the nonlinear model for the GC-MMC. Thus, expending positive and negative synchronous reference frames is vital. To achieve this goal, firstly, three-phase currents and voltages are measured. Then they are converted into their positive and negative sequence components, which are then served along with the reference current signals to generate the reference voltage signals for the Pulse-Width Modulation (PWM) regulator. A sequence separation scheme is implemented to remove positive and negative sequences [15].

3. Fuzzy-Sliding Mode Control of the Grid-Connected Modular Multilevel Converter

The proposed control strategy based on the fuzzy sliding mode approach for a renewable energy system, such as photovoltaic or wind power units, is illustrated by the block diagram in Figure 2. As illustrated, power-following and fault ride through control of the GC-MMC are two important concerns which should be satisfied by designing a proper control approach. Typically, for each renewable power source, the maximum power point tracker (MPPT) is employed to attain the maximum power at variations of climate conditions and load changes. Thanks to the robust

characteristics of sliding mode control (SMC) and the adaptive nature of fuzzy systems, it was possible to combine fuzzy control and SMC. This combination was employed to reduce the chattering problem of SMC and the results were found to be effective. A complementary control strategy for a voltage source converter based on positive and negative symmetrical components was introduced in Reference [19] to investigate the voltage sag ride-through. In this paper, this idea was extended for the MMC and is explained as follows:
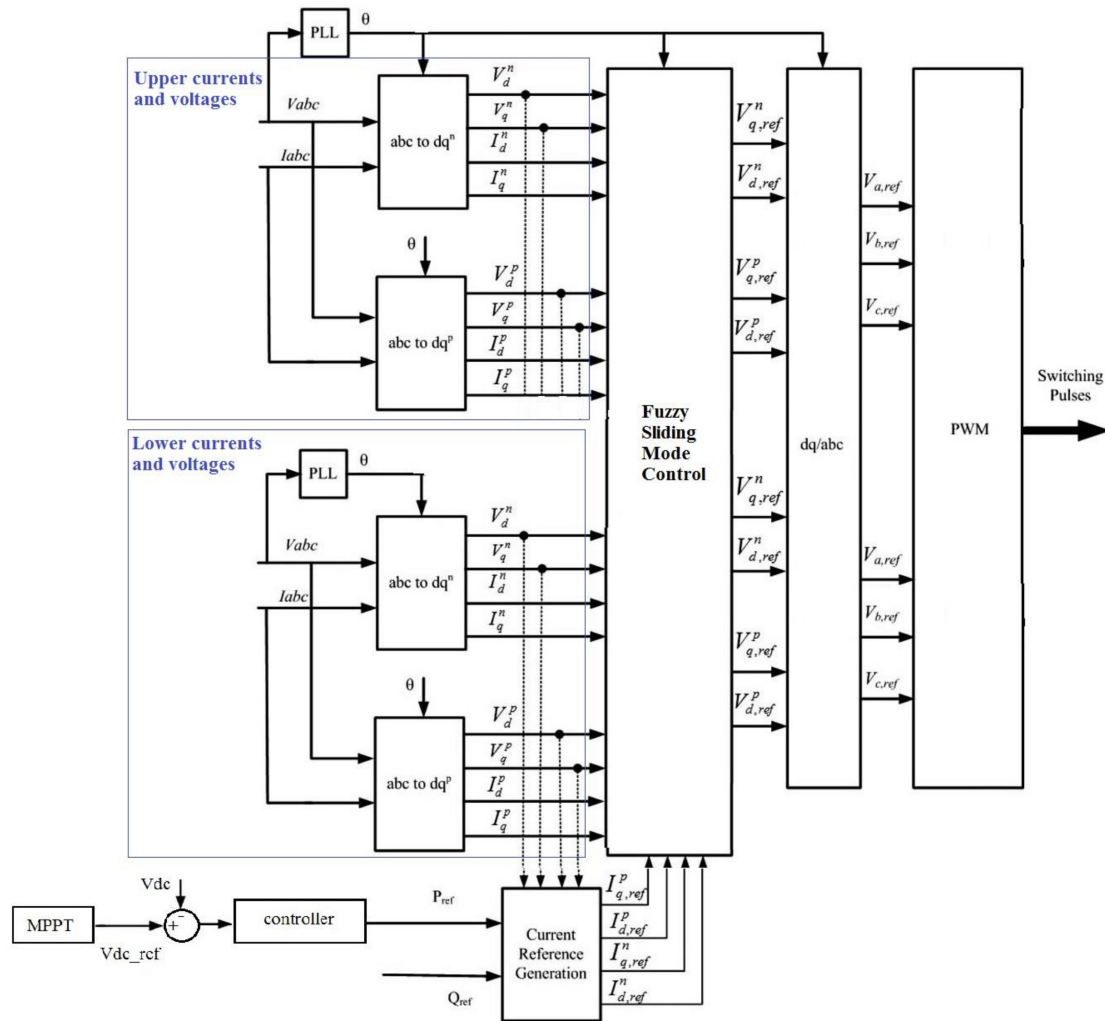

Figure 2. The proposed control strategy for the grid-connected MMC (GC-MMC).

The first part in the planning of the fuzzy sliding control strategy was describing the current tracking errors, which were realized for positive and negative sequence components as follows:

$$
\begin{aligned}
e_{dp}^{u} &= (i_{dp-ref}^{u} - i_{dp}^{u}) \\
e_{dn}^{u} &= (i_{dn-ref}^{u} - i_{dn}^{u}) \\
e_{qp}^{u} &= (i_{qp-ref}^{u} - i_{qp}^{u}) \\
e_{qn}^{u} &= (i_{qn-ref}^{u} - i_{qn}^{u}) \\
e_{dp}^{l} &= (i_{dp-ref}^{l} - i_{dp}^{l}) \\
e_{dn}^{l} &= (i_{dn-ref}^{l} - i_{dn}^{l}) \\
e_{qp}^{l} &= (i_{qp-ref}^{l} - i_{qp}^{l}) \\
e_{qn}^{l} &= (i_{qn-ref}^{l} - i_{qn}^{l})
\end{aligned}
\tag{2}
$$

where i^u_{dp}, i^u_{dn}, i^u_{qp}, i^u_{qn}, i^l_{dp}, i^l_{dn}, i^l_{qp} and i^l_{qn} are currents of symmetrical *dq* components which are defined for reference, upper and lower currents, respectively.

Commonly, after modulation, the next step is the activation and deactivation of a number of SMs. Therefore, an algorithm was developed for sorting the capacitor voltages of SMs. On that account, the voltage error between the SM capacitor voltages one step ahead and their references should be considered as follows:

$$e_j = \left| V_{c,j}(t + T_s) - V_{c,ref} \right| \tag{3}$$

where $V_{c,ref}$ is the reference SM capacitor voltage.

Then for each SM, the estimated capacitor voltage $V_{c,j}$ was obtained by the formula below:

$$V_{c,j}(t + T_s) = V_{c,j}(t) + \frac{i_{k,j}}{C} T_s \tag{4}$$

where $i_{k,j}$ is the arm current and T_s is the control time period.

Therefore, the concluding vector for forming the error matrix can be described as follows:

$$e = \begin{bmatrix} e^u_{dp} \\ e^u_{qp} \\ e^u_{dn} \\ e^u_{qn} \\ e^l_{dp} \\ e^l_{qp} \\ e^l_{dn} \\ e^l_{qn} \\ e_j \end{bmatrix}. \tag{5}$$

Then the sliding surface for the nonlinear system was written in Reference [18] as:

$$s(X(t), t) = \lambda e \tag{6}$$

where λ is a strict positive parameter which is regulated by the systems' bandwidth.

From this stage, the proposed control strategy was implemented as shown in Figure 2. The details of the fuzzy sliding mode control strategy are explained in Reference [20].

4. Simulation Results and Analysis

The entirety of the modeling of the MMC and the design of the control strategy were accomplished in MATLAB/Simulink software in order to monitor the system performance. The nominal parameters which were used for the simulation of power electronic converter and controller are shown in Table 1. The reference amounts for the real and reactive powers were defined and then applied. The steady-state performance of the MMC regulated by the fuzzy sliding mode control strategy was investigated in this set of tests.

The capacitor voltages which are related to upper and lower cells of Phase A are illustrated in Figure 3. Considering Equation (3), the control input made the SM voltage track the reference value (5892 V) properly, as depicted in Table 2. As observed, with the help of the proposed nonlinear control method, the MMC operated stably with balanced submodule capacitor voltages when the reference powers were applied. The three-phase line-to-line voltages are shown in Figure 4a, in which four levels of voltage are undoubtedly observable. It is noticeable that during the charging and discharging of the capacitors, the voltage levels varied within acceptable boundaries. The exploited MMC in this study was a conventional MMC and the simulation results obtained prove that the THD of the output voltage was around 7.56%, taking into consideration the ripple in the capacitor voltages. However, the

performance of the proposed control of the MMC showed a significant improvement in its reduction of the THD of the output voltage. Moreover, Figure 4b illustrates the AC side currents. As shown, they were balanced and stable during the fault conditions. The THD of the AC currents was less than 1%.

Table 1. Parameters for the simulation of the whole system.

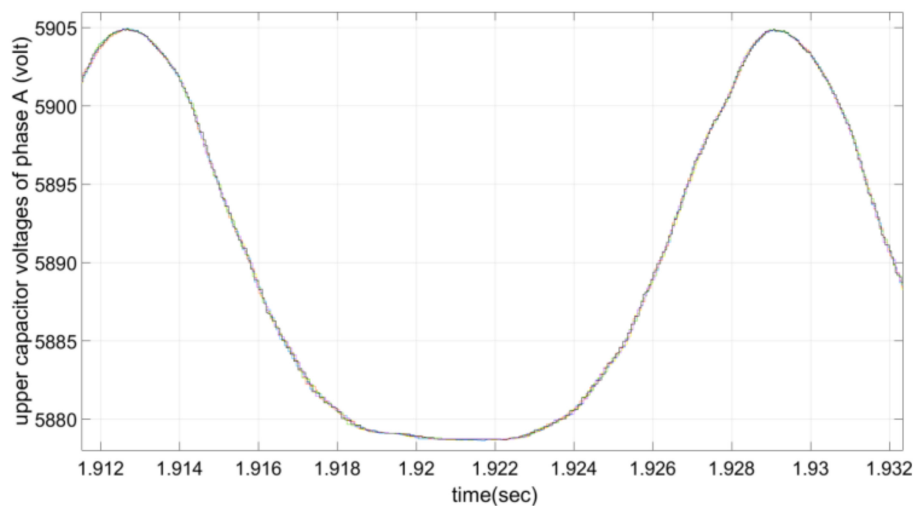| Nominal Parameters	
Submodule (SM) capacitor initial voltage	5892 V
Input DC voltage	20 kV
Rated line-to-line voltage	10 kV
Number of cells per arm	6
Arm inductance	1.59 mH
Arm resistance	0.04 mΩ
Cell capacitance	100 μF
Rated frequency	60 Hz
Carrier frequency	600 Hz
Real power reference	0.05 MW
Reactive power reference	0.2 MVAr

Figure 3. The upper capacitor voltages of Phase A.

Table 2. Parameters of power converters and controllers.

Arm inductance	5 mH
DC link voltage	20 V
Cell capacitance	3.3 mF
Rated frequency	50 Hz
Carrier frequency	2000 Hz
Sampling frequency	25 kHz

Figure 5 shows the Fast Fourier Transform (FFT) analysis of the output voltage under steady-state conditions. As can be observed, the multiples of second fundamental were significantly suppressed. Additionally, the THD was also reduced.

The circulating current of the leg in Phase A flow, which circulates through the arms and the DC side of the converter, is illustrated in Figure 6. Due to accurate stabilization of the SM voltage, the circulating current of MMC was suppressed and it balanced the power in the capacitors on the DC side of the MMC. The steady-state simulation confirmed the precise process of the MMC with the proposed technique.
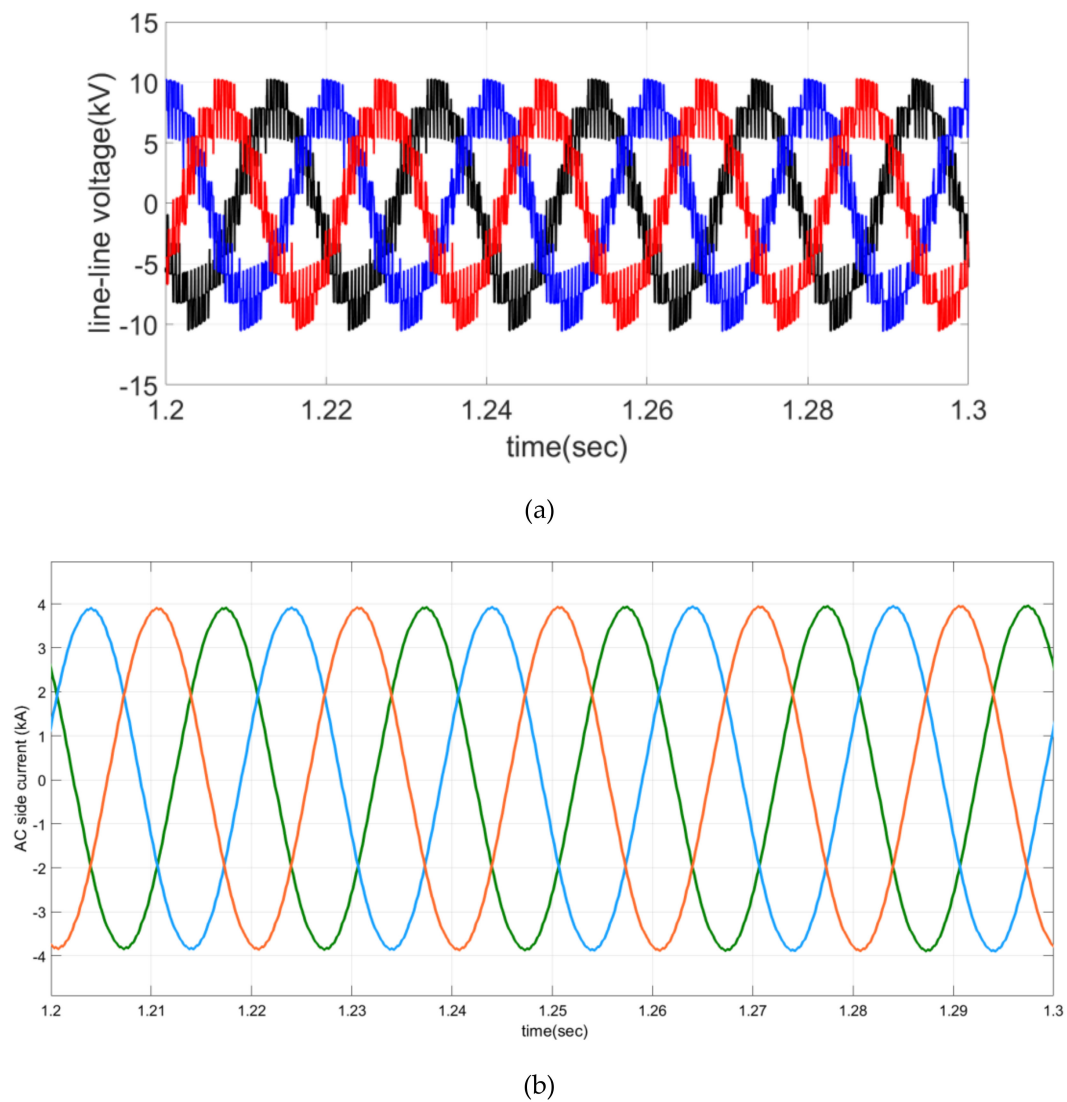
(a)

(b)

Figure 4. Three-phase voltages (**a**) and AC side currents (**b**).
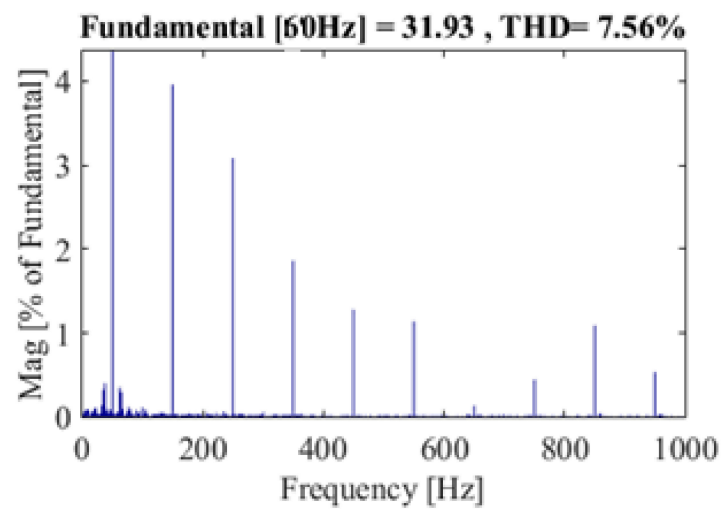

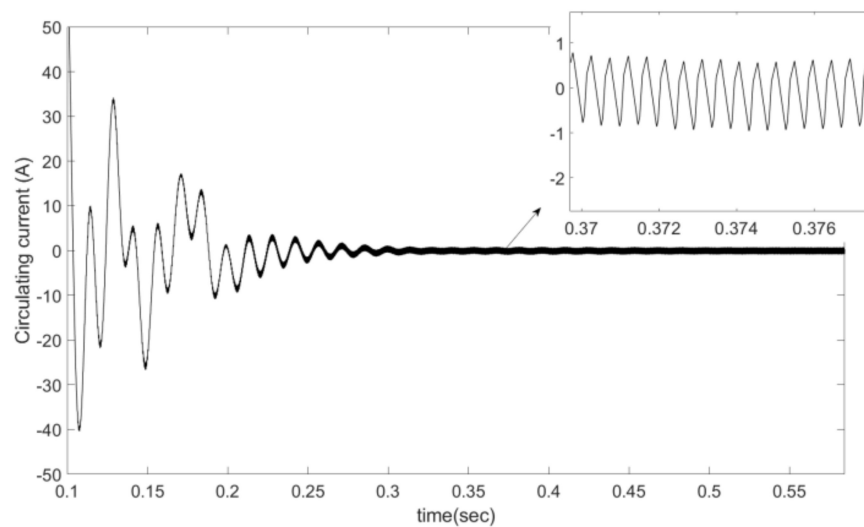**Figure 5.** Fast Fourier Transform (FFT) analysis of the output voltage.

Figure 6. The variations of circulating current.

Figure 7 demonstrates how the converter replied to the requested active power and reactive power. For this purpose, ramp-up and ramp-down changes were implemented in input power to simulate the behavior of changing the solar irradiation. In this case, the reactive power went up to 0.2 MVAr. It illustrated a matching change in the transferred active and reactive powers. There was also an improvement in the steady-state and transient responses while applying the proposed controller.
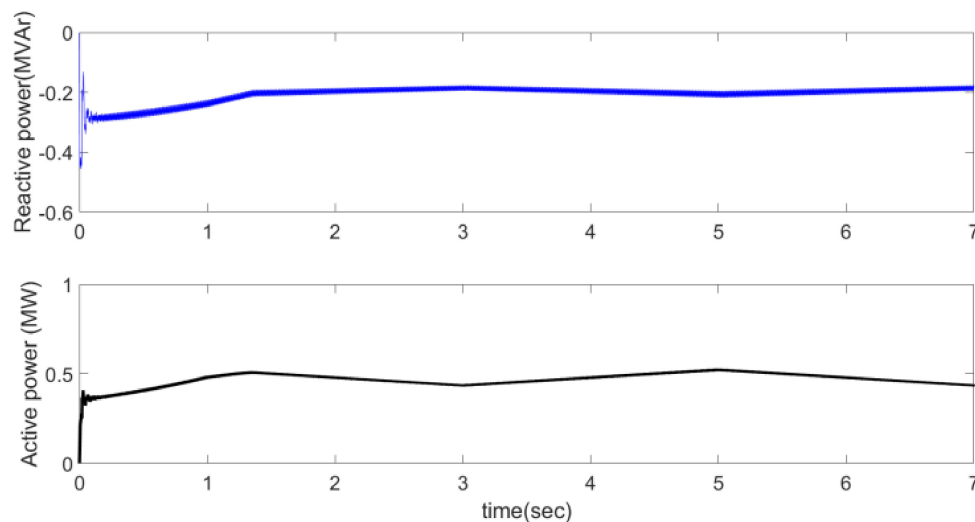

Figure 7. Dynamic response of the GC-MMC to the ramp-up and ramp-down changes of input power command.

Supplementary assessment of the proposed controller was performed during grid voltage disturbance. Case (a) (Type B voltage sag) considered a single-line-to-ground (SLG) fault of Phase A, whilst cases (b) and (c) considered a Type C and D sag down to 80% (voltage drops 20%). The specific unbalanced grid voltages and simulation results of cases (a)–(c) are shown in Figure 8.
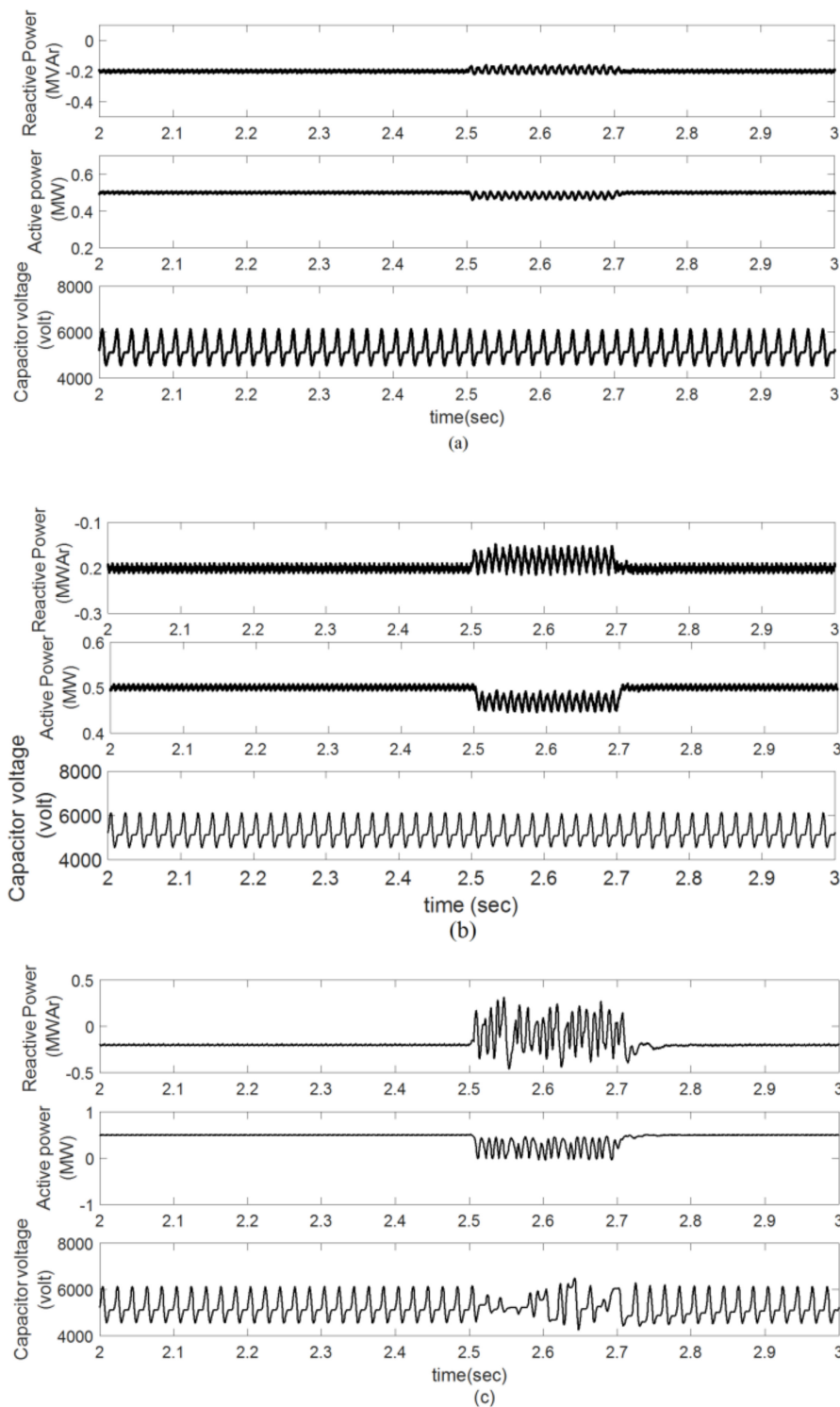
Figure 8. Time domain response of the GC-MMC during (**a**) unbalanced voltage sag due to a single-line-to-ground fault, (**b**) unbalanced voltage sag due to a line-to-line fault and (**c**) unbalanced voltage sag due to a double-line-to-ground fault.

In Phase A, voltage sag is considered to drop 20% at t = 2.5 s over 20 ms. In the beginning, the MMC was delivering 0.5 MW active power and 0.2 MVAr reactive power to the grid. As illustrated in Figure 8, there were oscillations in active and reactive powers during the unbalanced voltage fault. It is observable that the offered current controllers allowed sustained power as demanded by the DC power source during and after the fault. In spite of the imbalance of the AC voltages, the current

controller was able to balance the output AC currents. As a result, the active, alongside the reactive powers, started oscillating with the double frequency of an AC grid. Owing to the decoupling between the AC and DC parts, the voltage sag was compensated by the stored energy inside the MMC. Finally, as has been verified, the variation of capacitor voltages were within satisfactory bounds and were not influenced by grid voltage faults, excluding the voltage sag case (c). As illustrated in Figure 9c, the voltage sag due to the double-line-to-ground fault created many oscillations on the active and reactive powers, as well as many distortions of the capacitor voltage. In this situation, a supercapacitor with a high power density would be proposed to absorb the power oscillation during voltage sag and satisfy the voltage ride through condition at the output of the GC-MMC [19].
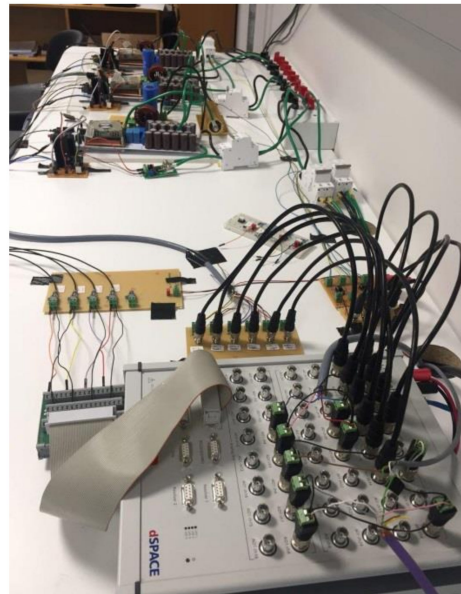

Figure 9. Setup of a three-level, single-phase MMC.

To observe the performance of the proposed controller, an experimental setup was developed. The test system was connected to a 750-W solar system. Since the system required many input/outputs and a sampling frequency up to 10 kHz, the dSPACE MicroLabBox was used as the real-time interface for the control of the MMC. The experimental setup consisted of a low-power MMC with three levels, as shown in Figure 9. The parameters of the experimental setup are listed in Table 2.

The MMC was examined under unbalanced voltage sag. The voltage waveform captured on the oscilloscope for the three-level MMC can be seen in Figure 10. The voltage waveform obtained on the oscilloscope had a peak voltage of approximately 10 V.
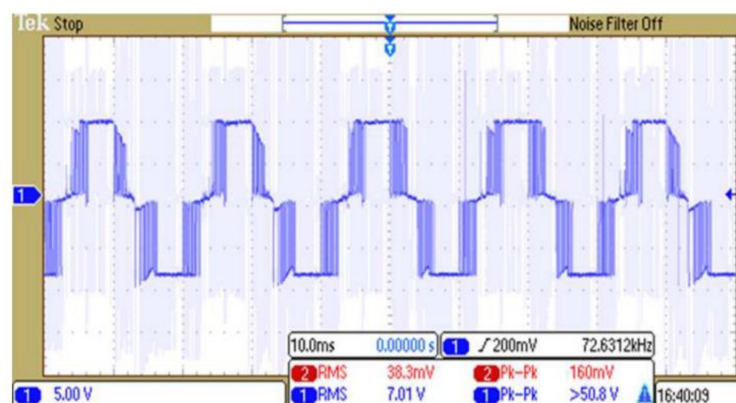

Figure 10. Voltage waveform across the load.

The voltage across the capacitor of module 1 as obtained on the control desk can be seen in Figure 11. As the voltage was obtained at $v_{dc} \approx 20$ V, it was expected that the average value when the algorithm is active, across any submodule, at any given time, should be approximately 10. The obtained results show that the MMC was stable under voltage sag condition and the proposed controller kept the capacitor voltage in the viable boundary.
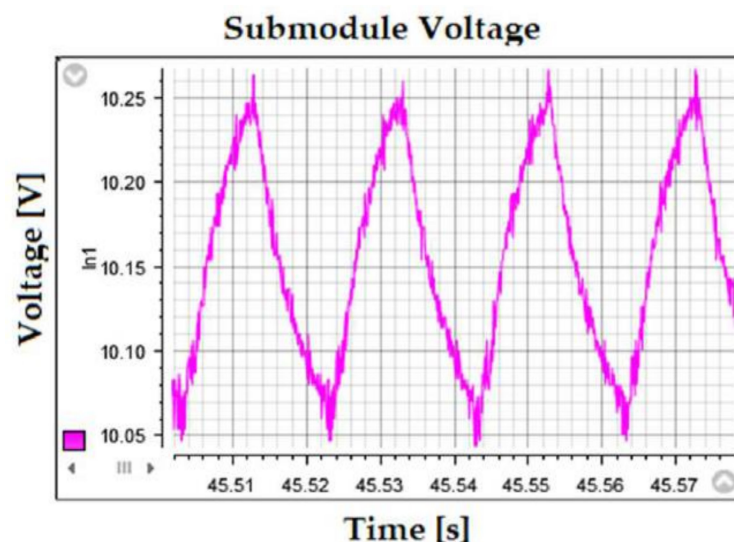

Figure 11. Capacitor voltage for submodule 1 obtained from the experimental setup.

5. Conclusions

This paper provided a robust current control strategy for the MMC. In view of the unbalanced voltage conditions and the complexity of the nonlinear model, a robust adaptive current control configuration, by means of sliding mode control and fuzzy control, was established for the GC-MMC. The planned control performed appropriately for the MMC and enabled separate control of the symmetrical elements of the grid currents. Additionally, the dynamic response of the MMC throughout voltage sag conditions and the effect of uncertainties on the filter parameters during changing power demands were evaluated numerically. The results specified that the current control strategy is more potent under voltage sag situations and able to fulfill the stability requirements of the MMC.

References

1. Wang, M.; Hu, Y.; Zhao, W.; Chen, G. Application of modular multilevel converter in medium voltage high power permanent magnet synchronous generator wind energy conversion systems. *IET Renew. Power Gener.* **2016**, *9*, 824–833. [CrossRef]
2. Alexander, A.; Thathan, M. Modelling and analysis of modular multilevel converter for solar photovoltaic applications to improve power quality. *IET Renew. Power Gener.* **2015**, *9*, 78–88. [CrossRef]
3. Mehrasa, M.; Pouresmaeil, E.; Taheri, S.; Vechiu, I. Novel Control Strategy for Modular Multilevel Converters Based on Differential Flatness Theory. *IEEE J. Emerg. Sel. Top. Power Electron.* **2018**, *6*, 888–897. [CrossRef]

4. Deng, F.; Chen, Z. Voltage-balancing method for modular multilevel converters under phase-shifted carrier-based pulse-width modulation. *IEEE Trans. Ind. Electron.* **2015**, *62*, 4158–4169. [CrossRef]

5. Mei, J.; Ji, Y.; Tian, J.; Huang, C.; Lu, X.; Du, X.; Xie, Y.; Hu, Q.; Ma, T. Balancing control schemes for modular multilevel converters using virtual loop mapping with fault tolerance capabilities. *IEEE Trans. Ind. Electron.* **2016**, *63*, 38–48. [CrossRef]

6. Lu, J.; Huang, Q.; Mao, X.; Tan, Y.; Zhu, S.; Zhu, Y. Optimized Design of Modular Multilevel DC De-Icer for High Voltage Transmission Lines. *Electronics* **2018**, *7*, 204. [CrossRef]

7. Siemaszko, D. Fast sorting method for balancing capacitor voltages in modular multilevel converters. *IEEE Trans. Power Electron.* **2015**, *30*, 463–470. [CrossRef]

8. Dekka, A.; Wu, B.; Yaramasu, V.; Zargari, N.R. Integrated model predictive control with reduced switching frequency for modular multilevel converters. *IET Electr. Power Appl.* **2017**, *11*, 857–863. [CrossRef]

9. Boecker, J.; Freudenberg, B.; The, A.; Dieckerhoff, S. Experimental comparison of model predictive control and cascaded control of the modular multilevel converter. *IEEE Trans. Power Electron.* **2015**, *30*, 422–430. [CrossRef]

10. Luo, L.; Zhang, Y.; Jia, L.; Yang, N. A novel method based on self-power supply control for balancing capacitor static voltage in MMC. *IEEE Trans. Power Electron.* **2017**, *33*, 1038–1049. [CrossRef]

11. Han, X.; Sima, W.; Yang, M.; Li, L.; Yuan, T.; Si, Y. Transient Characteristics Under Ground and Short-Circuit Faults in a ±500 kV MMC-Based HVDC System with Hybrid DC Circuit Breakers. *IEEE Trans. Power Deliv.* **2018**, *33*, 1378–1387. [CrossRef]

12. Abbassi, R.; Marrouchi, S.; Saidi, S.; Abbassi, A.; Chebbi, S. Optimal Energy Management Strategy and Novel Control Approach for DPGSs under Unbalanced Grid Faults. *J. Circuit Syst. Comp.* **2018**. [CrossRef]

13. Saidi, S.; Abbassi, A.; Chebbi, S. Fuzzy logic controller for three-level shunt active filter compensating harmonics and reactive power. *Int. J. Adapt. Control Signal Process.* **2016**, *30*, 809–823. [CrossRef]

14. Hajizadeh, A. Optimized thermal management system of Modular Multilevel Converter for HVDC applications. In Proceedings of the IMAPS Nordic Conference on Microelectronics Packaging (Nordpac), Gothenburg, Sweden, 4–6 April 2017.

15. Guzman, R.; de Vicuna, L.G.; Morales, J.; Castilla, M.; Matas, J. Sliding-mode control for a three-phase unity power factor rectifier operating at fixed switching frequency. *IEEE Trans. Power Electron.* **2016**, *31*, 758–769. [CrossRef]

16. Fang, Y.; Zhu, Y.; Fei, J. Adaptive Intelligent Sliding Mode Control of a Photovoltaic Grid-Connected Inverter. *Appl. Sci.* **2018**, *8*, 1756. [CrossRef]

17. Yang, Q.; Saeedifard, M.; Perez, M.A. Sliding Mode Control of the Modular Multilevel Converter. *IEEE Trans. Ind. Electron.* **2019**, *66*, 887–897. [CrossRef]

18. Li, A.; Xu, L.; Guo, D. Accelerated switching function model of hybrid. MMCs for HVDC system simulation. *IET Power Electron.* **2017**, *10*, 2199–2207. [CrossRef]

19. Hajizadeh, A.; Golkar, M.A.; Feliachi, A. Voltage Control and Active Power Management of Hybrid Fuel-Cell/Energy-Storage Power Conversion System Under Unbalanced Voltage Sag Conditions. *IEEE Trans. Energy Conver.* **2010**, *25*, 1195–1208. [CrossRef]

20. Ghiasi, M.I.; Golkar, M.A.; Hajizadeh, A. Lyapunov Based-Distributed Fuzzy-Sliding Mode Control for Building Integrated-DC Microgrid with Plug-In Electric Vehicle. *IEEE Access* **2017**, *5*, 7746–7752. [CrossRef]